Dear Author,

Please, note that changes made to the HTML content will be added to the article before publication, but are not reflected in this PDF.

Note also that this file should not be used for submitting corrections.

Nuclear Instruments and Methods in Physics Research A ∎ (∎∎∎∎) ∎∎∎–∎∎∎

Contents lists available at ScienceDirect

Nuclear Instruments and Methods in Physics Research A

journal homepage: www.elsevier.com/locate/nima

Gamma-ray inspection of rotating object

Tadashi Kambara *, Atsushi Yoshida, Hiroshige Takeichi [1]

RIKEN Nishina Center, 2-1 Hirosawa, Wako, Saitama 351-0198, Japan

ARTICLE INFO

Article history:
Received 30 January 2015
Received in revised form
8 May 2015
Accepted 14 June 2015

Keywords:
Radiotracer
Positron emission tomography
ML-EM algorithm
Image reconstruction
Rotating object

ABSTRACT

We develop a method to diagnose two-dimensional distribution of positron-emitting radioactivity in a rotating object through γ-ray coincidence measurements with two detectors. The principle of this method is same as PET but the measurement system is much simpler. We have constructed a prototype and performed tests with point-like and plate-shaped radioactive sources. The image reconstruction with ML-EM algorithm reproduced the distribution. It can be useful for radiotracer measurements of slow transport processes of materials in a closed system and can find applications in mechanical engineering.

1. Introduction

Radioisotopes (RIs) have long been used as tracers in many fields. In biology and medicine, radiotracers are used to study the transport and accumulation of specific elements or chemical compounds in living bodies. Imaging technologies such as positron emission tomography (PET) [1] or single-photon emission computerized tomography (SPECT) have been developed and utilized for non-invasive examination in hospitals. Radiotracers are also used in various fields of industry, which require real-time measurements of distribution of matter in closed systems like machines or plants without stopping the system. In such diagnoses, a radiotracer is added to the object material and the time dependence of the γ-ray intensity is monitored from outside. For example, the flow and mixing of fluids like gas, liquid or powder are measured in petroleum, chemical and mineral-processing industries[2,3], where radiotracers are injected to the fluid and monitored at downstream by radiation detectors. On the other hand, thin-layer activation (TLA) method is employed for diagnosis of wear or corrosion of solid materials of machine parts or piping, where a thin layer of the surface of the object is activated and the removal rate of the surface is determined by the measurement of the radioactivity [4,5].

In most of the industrial applications, the transfer of the radiotracers are monitored through the time dependence of the radiation intensity measured by detectors fixed at proper positions. If the time-dependent spatial distribution of the radioactivity is visualized by tomography methods like gamma camera, SPECT [3] and PET [6], it would be possible to obtain more details of the dynamical processes in the closed system.

We develop a new method to determine two-dimensional spatial distribution of positron-emitting RIs on rotating objects [7]. It is based on the same principle as medical PET systems but is simpler and less expensive. It would be useful in some industrial applications such as wear diagnostics of rotating parts in a machine. In Section 6, we discuss possibility to combine it with a new method of TLA with RI-beam implantation[8].

2. Method

A significant part of nuclear β^+ decay in matter is followed by emissions of two 511-keV γ-ray photons in almost opposite directions. If the positron is annihilated on a line connecting two γ-ray detectors (Line Of Response: LOR), these photons can be detected in coincidence. Collecting coincidence events on various LORs in different orientations, the spatial distribution of the radiotracer can be reconstructed. In conventional PET, the object of diagnosis is at rest, surrounded by hundreds of γ-ray detectors and a pair of detectors which capture 511-keV photons in coincidence determine an LOR.

In our method, two γ-ray detectors that determine an LOR are placed on both sides of the object of diagnosis with radiotracer.

* Corresponding author. Tel.: +81 48 467 9507; fax: +81 48 461 5301.
E-mail addresses: kambara@ribf.riken.jp (T. Kambara), kambara@ribf.riken.jp (A. Yoshida), kambara@ribf.riken.jp (H. Takeichi).
[1] Present address: Advanced Center for Computing and Communication (ACCC), RIKEN, 2-1 Hirosawa, Wako, Saitama 351-0198, Japan.

http://dx.doi.org/10.1016/j.nima.2015.06.023
0168-9002/© 2015 Published by Elsevier B.V.

The object continuously rotates and the detectors move in parallel relative to the rotation center so that the LOR scans the object in all directions.

Fig. 1 shows the geometrical concept of an example where a point RI source is fixed on a continuously rotating disk. A Cartesian coordinate (X,Y) is fixed to space and (x,y) is fixed to the disk with the origins of both at the center of the rotation. The position of the source is (r,θ) in the polar coordinate fixed to the disk. A pair of collimated γ-ray detectors on both sides of the disk determine the LOR on a line $X=s$. The detectors move back and forth in one body relative to the disk along the X-axis so that the LOR continuously scans the disk. Equivalently, the detectors may be fixed whereas the disk moves back and forth. In this case, the Cartesian coordinate (X,Y) is not fixed but moves back and forth with the rotation center of the disk.

The condition of coincidence detection of the two photons is expressed by an equation

$$s = r\cos(\theta+\phi), \tag{1}$$

where ϕ, the angle of the x-axis from the X-axis, shows the orientation of the disk. Therefore r and θ are fixed whereas s and ϕ change with time. When ϕ and s are scanned, the coincidence events from a point source fall on a sinusoidal curve in the ϕ–s plane, as shown in Fig. 2.

The sinusoidal curve represents the position of the source: its amplitude is equal to r and the angle ϕ at the maximum s is equal to $-\theta$. The ϕ–s plot of the coincidence event rate distribution is called sinogram.

For multiple point sources, the sinogram consists of multiple sinusoidal curves and if the source has a two-dimensional distribution on the disk, the corresponding sinogram is a superposition of sinusoidal curves weighted by the radioactivity distribution. Conversely, when a sinogram is given, the two-dimensional spatial distribution of the source can be reconstructed. Therefore, with only two detectors, the RI distribution on a continuously rotating object can be inspected, if s and ϕ at the time of coincidence detection are determined.

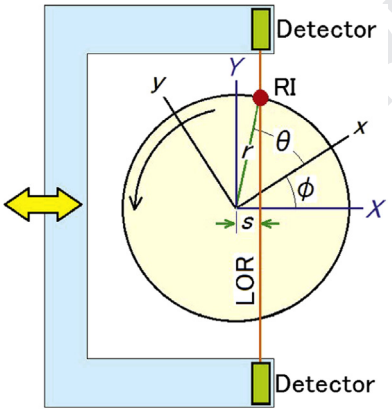

Fig. 1. Geometrical concept. The two detectors move as one body in X-direction.

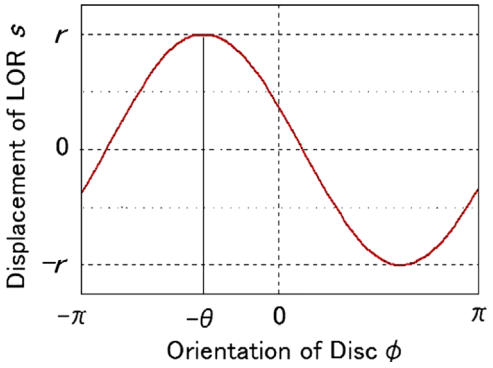

Fig. 2. Sinogram for one point source.

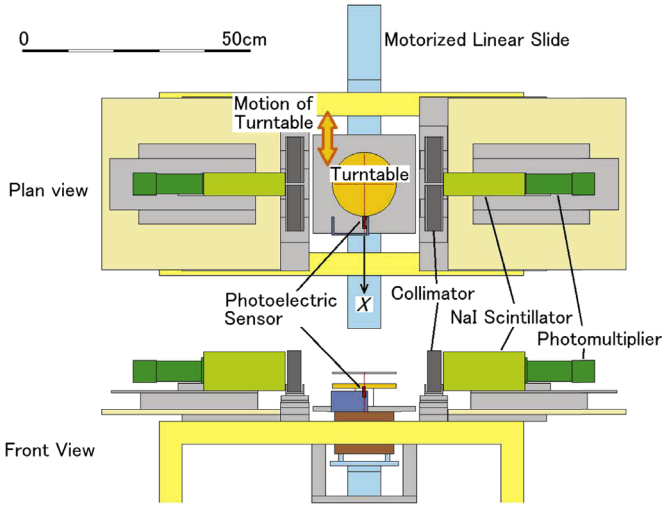

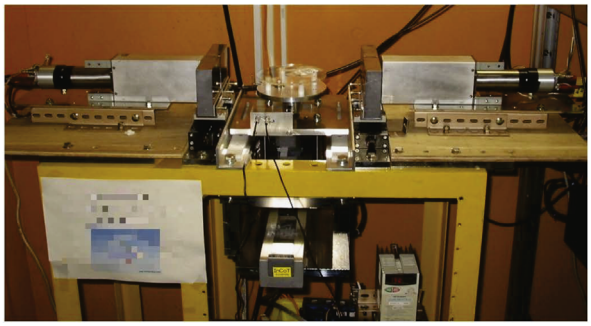

Fig. 3. The setup (upper) and photograph (lower) of the prototype.

3. Prototype

In order to prove the feasibility of the method, we have constructed a prototype. Fig. 3 shows the setup (upper) and the photograph (lower). A turntable with a diameter of 14 cm holds RI sources. The turntable is a plastic disk supported by plastic pillars so that the attenuation of γ rays is minimized. A pair of rectangular-shaped NaI-scintillator detectors (Saint Gobain Crystals and Detectors, 1.77×3.15H6.3/1.5L-X, 45 mm wide, 80 mm high and 160 mm deep) are placed on either side of the turntable opposite to each other. A pair of 3-cm thick Pb blocks are placed in front of each detector to form a vertical aperture for a γ-ray collimation. The center lines of the scintillators and the apertures of the collimators are aligned to a common line which determines the LOR.

In order to scan the turntable with LOR, the rotating turntable is mounted on a motorized linear slide and moves back and forth perpendicular to the LOR between the NaI detectors. The displacement of the LOR relative to the center, s, is changed stepwise between -70 mm and 70 mm relative to the rotation center. For the measurement of the orientation of turntable ϕ, a timing pin fixed to the turntable passes once per a turn through a photosensor fixed near the edge of the turntable. A timing pulse from the photosensor resets a clock-pulse scaler and the angle ϕ at the time of coincidence detection is deduced from the clock-pulse count.

The Cartesian coordinates in Fig. 1 are placed so that the X-axis is on a line from the rotation center through the photosensor and the x-axis is on a line from the center through the timing pin.

4. Test measurements

We have performed test measurements with the prototype to evaluate the sensitivity, spatial resolution and signal-to-noise ratio. We report here two examples where ^{22}Na sources were used. In the first example, we used two point-like sources of 1.55 and 65 kBq as shown in lower right of Fig. 6. The size of the point-like sources were evaluated with an imaging plate and the full width at half maximum of the RI distribution was about 1 mm for the 1.55-kBq source and 2 mm for the 65-kBq source. In the second example, we used a 6 cm × 10 cm rectangular Al-plate on which radioactivity of 149-kBq was distributed around a 3.5 cm-diameter circular hole at the center. The photograph of the turntable and the radioactivity distribution of the plate source taken by an imaging plate (BAS IP MS2040E, GE Healthcare) are shown in the left and middle of Fig. 9, respectively.

In both cases, the aperture of the Pb collimators was 6 mm and the distance between the opposing collimators was 276 mm. The turntable continuously rotated at 150 rpm (400 ms/turn) and moved back and forth by 2-mm step per about 10 s over $s = \pm 70-$mm range so that the LOR scans over the whole turntable in 714 s. The timing pin for the measurement of ϕ is at the right-hand side of the turntable in the photographs in Figs. 6 and 9. A scaler counts continuous 500-Hz pulses from a clock generator and is reset by the signal from the photosensor at each turn of the turntable. Therefore one turn corresponds to 200 pulses and the resolution of ϕ was 1.8°. At each coincidence detection of two 511-keV photons, the clock-pulse count and the position of the slide as well as the pulse heights from the both scintillation detectors were collected by a CAMAC-based system and recorded on a personal computer in list mode. In the analyses of the data, the true coincidence events were identified as the detection of 511 keV photons by the both detectors. More than 99.9% of ^{22}Na decay is accompanied by a 1275-keV γ-ray from the de-excitation of the daughter nuclide ^{22}Ne, but the photopeak of the 1275-keV photons was well separated in the pulse-height measurement and did not affect the analyses.

The measurement with the point-like sources collected 7.8×10^4 true-coincidence events in about 24 h with a coincidence rate of 0.89 Hz, and that with the plate source collected 1.18×10^5 events in about 24 h with a rate of 1.35 Hz. The accumulated events were sorted according to ϕ and s to obtain sinograms.

Fig. 4 shows the sinogram from the point-like sources on the left and that from the plate source on the right. The sinogram of the point-like sources shows two sinusoidal curves which correspond to the two sources and that of the plate source shows two broad bands with sinusoidal shapes which correspond to two regions of dense RI distribution on the plate. The RI distributions have been derived from these sinograms with a reconstruction algorithm described in the next section.

5. Reconstruction of RI distribution

5.1. Algorithm

To reconstruct the two-dimensional RI distribution from the sinogram, we use the maximum likelihood – expectation–maximization (ML-EM) algorithm [9] that is established and widely used in PET image reconstruction. The calculations for the reconstruction were performed by a program written in VEE Pro (Agilent Technologies) on a personal computer.

ML-EM is an iterative method whose detail is described in Ref. [9]. Here we present a simple explanation of the algorithm according to our setup using Figs. 1 and 5. We assume a two-dimensional RI distribution $\lambda(x, y)$ on the rotating object where (x, y) is the coordinate fixed to the object. $\lambda(x, y)$ is called image hereafter. The corresponding sinogram $p(\phi, s)$ where ϕ is the angle of the y-axis from the LOR and s is the displacement of the LOR from the rotation center. $p(\phi, s)$ is called projection hereafter.

The iteration starts with an arbitrary image that is updated gradually as

$$\lambda_j^n = \frac{\lambda_j^{n-1}}{\sum_i c_{ij}} \left(\sum_i \frac{c_{ij} p_i}{\sum_k c_{ik} \lambda_k^{n-1}} \right) \quad (2)$$

where λ_j^n is the jth pixel value in the image λ of the nth iteration, p_i is the value at the ith position in the projection p, and c_{ij} is a coefficient matrix element which is the probability that a γ-ray emitted from the jth pixel position is counted at the ith position in the projection.

The conventional image reconstruction algorithm in PET is filtered back-projection (FBP) in which projections from all angles are back-projected onto and overlaid in the image plane using the inverse Radon transform. ML-EM is advantageous over FBP for applications in that the image values are all non-negative and the signal-to-noise ratio is higher. Actually, FBP image of a strong RI source is accompanied by a starburst-like pattern which may hide weak sources around it. Further, ML-EM is more suitable for quantitative evaluation because the sum of the image values is preserved during the iteration and the γ-ray attenuation in the machine and collimators can be implemented in c_{ij}.

The coefficient matrix elements c_{ij} depend on the coincidence detection efficiency of the detectors and the attenuation of γ rays by materials between the source and the detectors. We neglected the attenuation by the pillars of the turntable and assumed that

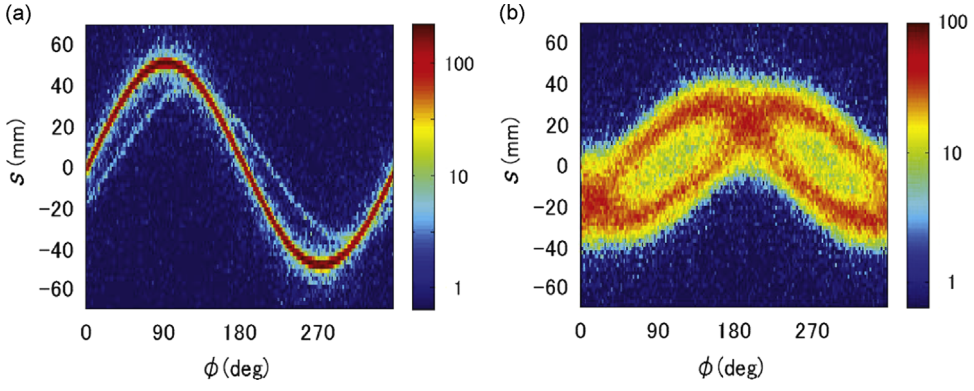

Fig. 4. Sinogram from two point-like sources (left) and a plate source (right).

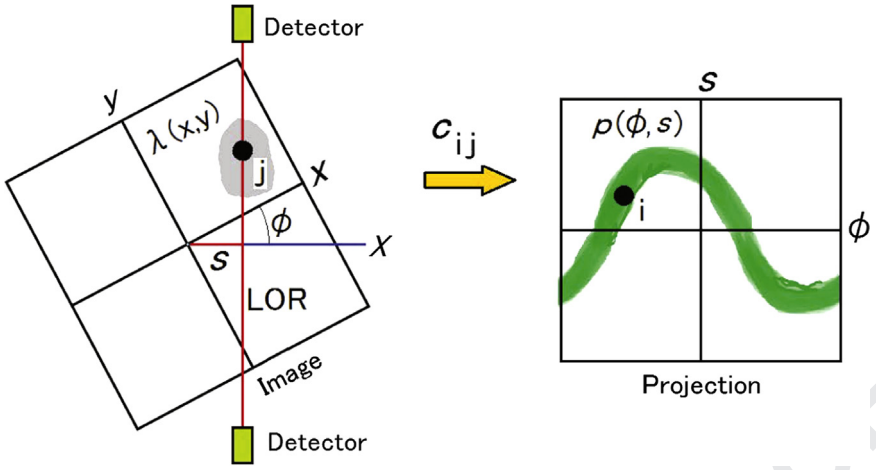

Fig. 5. Schematic illustration of image reconstruction by ML-EM algorithm.

the system was rotationally symmetric. Then c_{ij} was a function of the position of the source relative to the detectors. We used the 65-kBq point-like ^{22}Na source to measure the coincidence rate along the center line of the LOR at 10-mm intervals and that across the LOR at 0 mm, 40 mm and 70 mm from the center. A geometrical model function well reproduced the efficiency distribution across the LOR. So we weighted the model function by the measured coincidence efficiency on the center line, averaged it over the collimator width of 6 mm and used the result as the c_{ij} along the LOR. For simplicity, the c_{ij} was set non-zero only within the width of a pixel (2 mm). We are pursuing to evaluate the c_{ij} more precisely.

5.2. Results

The reconstructed images of the RI distributions have a pixel size of 2 mm × 2 mm. From the initial uniform image, iteration of 20 steps in the ML-EM was enough for point-like sources, but about 100 steps were required for the plate source. We judged the convergence by the appearance of the image.

5.2.1. Point-like sources

Fig. 6 shows the RI distribution for the case with two point-like sources. A two-dimensional image on the upper-left and the photograph of the turntable on the lower right are with the same size and orientation. The projections of the distribution to the x and y axes are shown in the lower left and upper right diagrams.

The two-dimensional image and the photograph show the outline of the turntable and the positions of the sources by red circles. The 65 kBq and 1.55 kBq sources are identified on the image and their positions are reproduced within a few millimeters. The ratio of their total intensities on the image is 40.1 which is close to the ratio of their radioactivities of 41.8. The full width at half maximum (FWHM) of the higher peak is about 4.2 mm in the x direction and 3.3 mm in the y direction. When a point source is imaged by γ-ray collimators with 6-mm of aperture, the FWHM of the image would be 3 mm. Therefore the width of the image of the point source seems mainly due to the collimator aperture. The width of the reproduced peak appears different between the x- and y-directions, but actually it is a difference between the r- and θ-directions as confirmed by measurements with different source positions. As shown in Fig. 2, the r and θ components of the image correspond to the amplitude and phase of the sinogram and their resolutions could be different by the measurement conditions or the image reconstruction algorithm. The source of the difference is so far not clear. The tail of the peak extends by about 20 mm which may be due to the penetration of γ rays at the edge of the collimator. The background intensity outside the tail is below 2×10^{-4} of the peak intensity.

As shown in Fig. 2, the rotation center $s=0$ is the base line of the sinusoidal curve in the sinogram. The position of the detectors on the X-axis should be calibrated so that the rotation center is at the origin $s=0$. The FWHM of the reconstructed peak from a point source increases with the deviation of the origin from the rotation center and the image becomes ring-shaped when the deviation exceeds about 2 mm. Therefore, by searching the minimum FWHM in the image reconstruction, the position of the detectors on X-axis was calibrated within ± 0.2 mm.

We studied the dependence of the sensitivity and spatial resolution on the number of the coincidence events by analyzing the list-mode data for different numbers of scans of the LOR. One scan took 714 s and collected about 640 coincidence events. Fig. 7 demonstrates the change of the reconstructed images of the two point-like sources with the accumulation of the events. The higher peak is clearly reconstructed within two scans (24 min), but the lower peak is obscure below 10 scans (2 h). Fig. 8 shows the convergence the x-direction FWHM of the higher peak and the ratio of the intensities between the higher and the lower peaks, as functions of the number of the coincidence events. The width of the higher peak is reconstructed well by about 1300 events and the ratio converges at about 26,000 coincidence events, which took about 8 h.

5.2.2. Plate source

Fig. 9 shows the RI distribution for the plate source. A photograph of the turntable is on the left, the RI distribution of the plate source taken with an imaging plate is at the center, and the reconstructed image with the ML-EM is on the right. The red lines in the photograph and gray lines in the image show the outlines of the turntable and the plate source with a hole at the center.

The overall structure of the RI distribution is well reproduced in the reconstructed image. Although there is no RI in the 35 mm-diameter hole at the center of the plate, both of the imaging plate and the ML-EM images show some distribution in the hole. This filling of the hole may partly be due to stray positrons from the edge of the hole. In addition, the filling looks more noticeable for imaging plate that is sensitive to β^+ and γ-rays, while the ML-EM reconstruction is sensitive to the positron distribution only.

Please cite this article as: T. Kambara, et al., Nuclear Instruments & Methods in Physics Research A (2015), http://dx.doi.org/10.1016/j.nima.2015.06.023

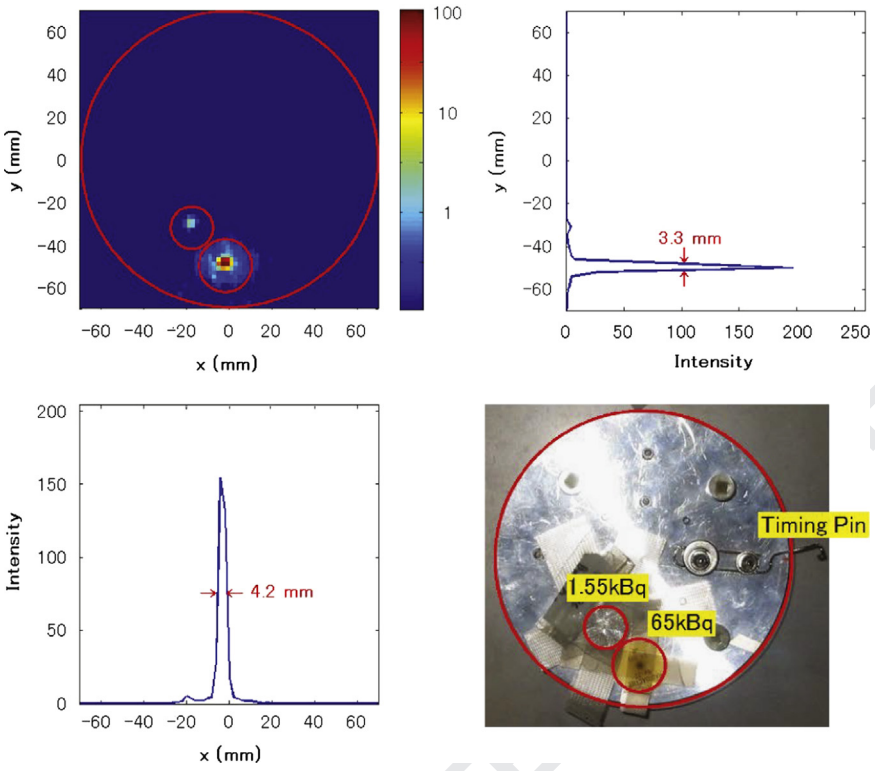

Fig. 6. Reconstructed RI distribution for the case with two point-like sources: the two-dimensional image of the RI distribution is shown in upper left and its projections on x- and y-axes are shown in the lower left and upper right, respectively. A photograph of the turntable is shown in the lower right. Red circles in the two-dimensional image and the photograph show the outline of the turntable and the positions of the sources. (For interpretation of the references to color in this figure caption, the reader is referred to the web version of this paper.)

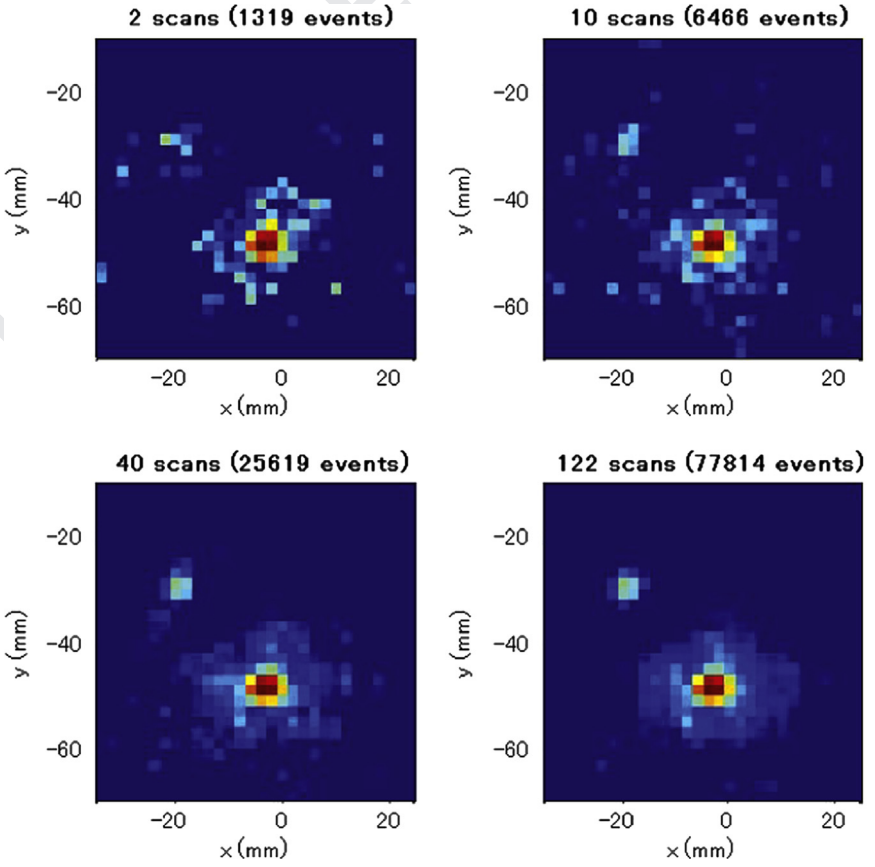

Fig. 7. Image of the peaks reconstructed from sinograms taken during 2, 10, 40 and 122 scans of LOR. The number of the coincidence events are also shown.

Please cite this article as: T. Kambara, et al., Nuclear Instruments & Methods in Physics Research A (2015), http://dx.doi.org/10.1016/j.nima.2015.06.023

The ML-EM image shows some background outside of the plate source, and the background intensity relative to the source is higher than that of the point-like sources. A point-like source gives a thin sinusoidal curve on its sinogram but a plate source gives two-dimensional distribution with a higher statistical variation of counts on the sinogram. It may cause the background in the reconstruction process. Although it appears that there is no background outside the turntable, it is merely because the values of c_{ij} in Eq. (2) were set to zero in this region.

6. Discussions

We describe the background and motivation of the development of this method which we name here GIRO (Gamma-ray Inspection of Rotating Object), compare it with conventional PET and evaluate possibilities of practical applications to TLA.

Before development of GIRO, we had been developing radioactive-isotope beam (RI-beam) implantation [8] as a new thin-layer activation (TLA) method for wear diagnostics of mechanical parts. With in-flight RI-beam separators at RIKEN, we can implant high-purity RI tracers at the surface of the diagnosed object with a controlled depth profile. We assumed that possible customers of this new TLA method would be in the engines and power transmission industries. In these fields, they evaluate the wear through γ-ray measurements during continuous operation of the machine: they determine the degree of wear by the decrease of the radioactivity of the object machine part or the increase of the radioactivity in the lubricant. Therefore, they need a lubricant circulation system to remove the activated debris from the machine to the outside. However, in some cases, it is not easy to install a circulation system for this purpose.

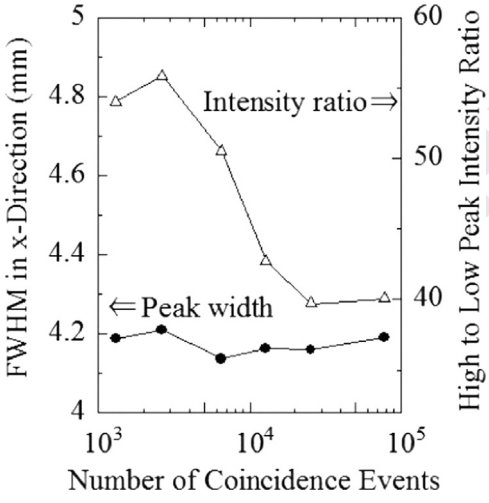

Fig. 8. The *x*-direction FWHM of the higher peak and the ratio of the higher peak to the lower one as functions of the number of the coincidence events.

We searched for optimum tomography methods for these cases and devised a way to utilize the continuous rotation of the object with minimal composition of detectors. Even when an activated debris remains in the closed system, its motion becomes out of phase from the originally activated parts and we can distinguish the wear-loss debris from the remaining activity with the tomography.

GIRO setup is smaller, lighter, and cheaper than conventional PET and can easily be transported in actual working places like factories. The diagnosed object in PET is surrounded by detectors and its size is limited by the bore of the instrument, but GIRO has more flexibility in the size and shape of the diagnosed object since it should only fit between a pair of detectors and its sizes in other directions are not limited. Since the object should continuously rotate, GIRO seems not suitable for diagnosis of living bodies. However, if the object has an intrinsic rotation, or the object can be mounted on a rotating turntable, the GIRO method is easily applicable. Measurements in nearly static conditions would be possible with quick scan and slow rotation. GIRO can be useful not only to measure fixed RI distributions in an object, but also to diagnose dynamical processes occurring in the object. A downside of GIRO is a lower detection efficiency than usual PET. Therefore GIRO is suitable for slow transport processes of matter like wear of mechanical parts, slow chemical reactions or motion of highly viscous liquids if radiotracers with sufficiently long lifetime are used.

Using our new TLA method mentioned above, we have achieved about 170 kBq of ^{22}Na implantation in materials. If this amount of ^{22}Na is implanted in a rotating machine part, according to our estimation, GIRO can image the daily change of the RI distribution to diagnose the wear. In the case of a closed system, the reconstructed image at any time can be normalized to the total amount of radioactivity calculated from the implanted activity and the natural decay half-life.

7. Conclusions

We present a method (GIRO) to inspect a two-dimensional distribution of positron-emitting RI with a minimal composition of γ-ray detectors. It consists of a continuously rotating object with RI and collimated two γ-ray detectors on both sides of it. The detectors and the object are in a continuous relative linear motion,

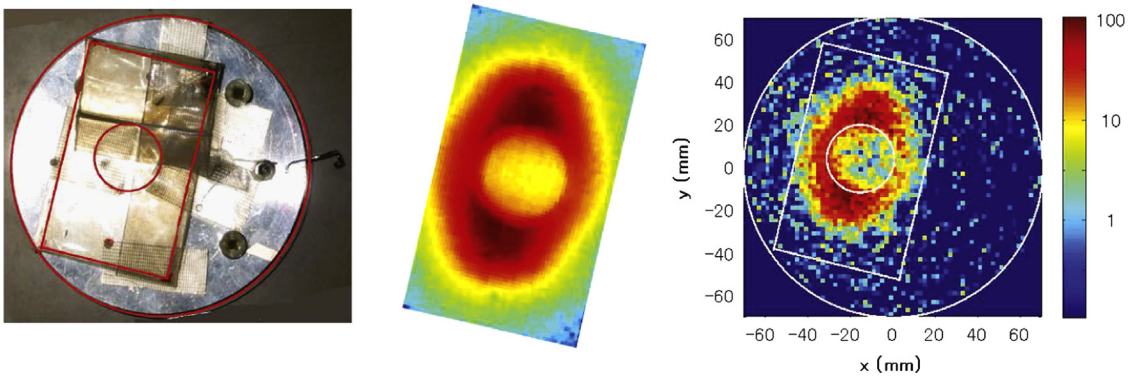

Fig. 9. Left: Photograph of the turntable with the plate source. Center: RI distribution on the plate source taken with an imaging plate. Right: Image of RI distribution reconstructed by ML-EM algorithm. The outlines of the turntable and the plate source are shown by lines in the reconstructed image and photograph. (For interpretation of the references to color in this figure caption, the reader is referred to the web version of this paper.)

and the coincidence γ-ray detection events are recorded with the object orientation and the position of the relative motion. GIRO is in principle same as conventional PET.

We have made measurements with a prototype setup, obtained sinograms and reconstructed images with the ML-EM algorithm. We have achieved a spatial resolution of about 4 mm in FWHM with a point-like ^{22}Na source, and reproduced a two-dimensional RI distribution.

Further developments including quicker scan, different rotation rates, and refinement of the ML-EM algorithm are progressing. We are aiming to utilize this method for a wear diagnostics of actual mechanical parts like gears or shaft drives in a running machine.

Acknowledgements

The authors are grateful to the members of RIKEN Nishina Center for various technical helps and for lending the NaI detectors. The motorized linear slide was fabricated by G-Tech company. This study is supported by NSK Foundation for Advancement of Mechatronics.

References

[1] P. Zanzonico, Seminars in Nuclear Medicine 34 (2004) 87.
[2] International Atomic Energy Agency, Radiotracer technology as applied to industry, IAEA-TECDOC-1262, Vienna, 2001.
[3] International Atomic Energy Agency, Radiotracer Applications in Industry—A Guidebook: Technical reports series, No. 423, Vienna, 2004.
[4] D.C. Eberle, C.M. Wall, M.B. Treuhaft, Wear 259 (2005) 1462.
[5] P. Fehsenfeld, C. Eifrig, R. Kubat, Nuclear Physics A 701 (2002) 235c.
[6] D.J. Parker, T.W. Leadbeater, X. Fan, M.N. Hausard, A. Ingram, Z. Yang, Measurement Science and Technology 19 (2008) 094004.
[7] Japan Patent Application No. 2014-034417.
[8] A. Yoshida, T. Kambara, A. Nakao, R. Uemoto, H. Uno, A. Nagano, H. Yamaguchi, T. Nakao, D. Kahl, Y. Yanagisawa, D. Kameda, T. Ohnishi, N. Fukuda, T. Kubo, Nuclear Instruments and Methods B 317 (2013) 785.
[9] L.A. Shepp, Y. Vardi, IEEE Transactions and Medical Imaging 1 (1982) 113.

Please cite this article as: T. Kambara, et al., Nuclear Instruments & Methods in Physics Research A (2015), http://dx.doi.org/10.1016/j.nima.2015.06.023